Stoichiometry and discommensuration on $In_xGa_{1-x}As/GaAs(001)$ reconstructed surfaces: A quantitative x-ray diffuse-scattering study

Y. Garreau* and K. Aïd
LURE Centre Universitaire Paris-Sud, Bâtiment 209D, Boite Postale 34, 91898 Orsay Cedex, France

M. Sauvage-Simkin
LURE Centre Universitaire Paris-Sud, Batiment 209D, Boite Postale 34, 91898 Orsay Cedex, France and Laboratoire de Minéralogie-Cristallographie, associé au CNRS et aux Universités Pierre et Marie Curie (Paris 6) et Denis Diderot (Paris 7), 4 place Jussieu, 75252 Paris Cedex, France

R. Pinchaux
LURE Centre Universitaire Paris-Sud, Bâtiment 209D, Boite Postale 34, 91898 Orsay Cedex, France and Université Pierre et Marie Curie, 4 place Jussieu, 75252 Paris Cedex, France

C. F. McConville
Department of Physics, University of Warwick, Coventry, CV4 7AL, United Kingdom and Semiconductor Materials IRC, Imperial College, London SW7 2AB, United Kingdom

T. S. Jones
Semiconductor Materials IRC, Imperial College, London SW7 2AB, United Kingdom and Department of Chemistry, Imperial College, London SW7 2AY, United Kingdom

J. L. Sudijono and E. S. Tok
Semiconductor Materials IRC, Imperial College, London SW7 2AB, United Kingdom

(Received 16 July 1998)

A quantitative estimate of the In/Ga surface concentration ratio in ultrathin (In, Ga)As strained layers, grown by molecular-beam epitaxy on a GaAs(001) substrate, is obtained using grazing incidence x-ray diffraction and diffuse-scattering measurements. The commensurate 2×3 reconstruction is interpreted as due to cation ordering in the surface unit cell, locking the surface composition at the value $In_{2/3}Ga_{1/3}As$. Incommensurate $2\times n$ reconstructions with $n<3$ ($n>3$) are described in terms of indium-depleted (-enriched) surface layers characterized by a statistical distribution of faults in the ideal 2×3 atomic arrangement. Within a defined temperature range 450–490 °C, a unique correspondence between the incommensurability parameter n and the indium surface fraction is established on the basis of a formulation of the diffuse scattering distribution. [S0163-1829(98)04648-7]

I. INTRODUCTION

A reliable estimate of the surface stoichiometry in a multielement material is a crucial issue in surface science, and a large amount of work has been performed on metallic surface alloys.[1] Such information is needed particularly for heteroepitaxial growth, where interdiffusion or surface segregation processes are known to take place. In the case of (In, Ga)As-based III-V semiconductor heterostructures, which is of major technological interest, the experimental evidence for In surface segregation during growth and for the associated composition gradient has been obtained by a variety of methods including Auger and photoelectron spectroscopies[2,3] and photoluminescence.[4,5] The structures investigated consisted mostly of ternary layers with a low indium concentration fully strained on GaAs(001) substrates, or alternately of ultrathin InAs layers buried under a GaAs cap. The indium concentration in the top layers of $In_xGa_{1-x}As$ alloys was consistently found to be enriched compared to the nominal bulk value, and close to 0.7 in most cases.[2,3] For buried layers, indium could still be detected at the surface after the deposition of more than 10 ML of the capping material.[5] Furthermore, specific surface reconstructions, 2×3 or incommensurate $2\times n$, where $2.5<n<3$, were found on these alloy surfaces, which had not previously been observed in the binary compounds, GaAs or InAs. A clue to this correlation between surface reconstruction and surface composition has been obtained through the identification of the surface structure in the 2×3 unit cell by means of surface x-ray diffraction.[6] The ordering in the outermost (In, Ga) atomic layer was shown to lock the surface composition at a value of $In_{2/3}Ga_{1/3}As$. Furthermore, crystallographic analysis demonstrated the uniqueness of this structural arrangement for all (2×3)-reconstructed surfaces obtained on bulk alloys, in shallow buried interfaces, or even within submonolayer InAs deposits on GaAs, provided that a sufficient amount of indium could be brought to the surface.[7] The commensurate 2×3 arrangement could therefore be considered as an equilibrium surface for the fully strained (In, Ga)As surface alloy. Departures from this ideal arrangement, resulting in the

incommensurate $2\times n$ reconstructions, first studied in Ref. 8, have been assigned to the presence of indium depleted faults, in a previous structural assessment by x-ray diffraction.[6] On the basis of this model, a correlation was proposed between the parameter n and the surface indium concentration with the assumption of a homogeneous distribution of indium. However, in a recent study of InAs deposition on $c(4\times4)$ reconstructed GaAs, by scanning tunneling microscopy (STM),[9,10] it was demonstrated that the competition between surface diffusion and vertical exchange leads either to indium clustering (leaving bare GaAs surfaces) or to homogeneously covered (In, Ga)As alloy surfaces, depending on the deposition temperature.

The purpose of the present work is to establish clearly the link between the surface reconstruction and composition using a series of samples prepared *in situ* by deposition of submonolayer coverages of InAs on GaAs(001). Deposition was performed at temperatures high enough to avoid clustering and to produce incommensurate surfaces not studied yet with $n>3$. The commensurate 2×3 surface is intermediate between In-depleted and In-enriched surfaces, and its importance to the understanding of this series of structures is thus emphasized. A mathematical formalism giving an optimal account of the experimental diffuse scattering features observed in the surface x-ray-diffraction data is also presented.

II. EXPERIMENT

A. Sample preparation

The samples studied in this work were prepared by the deposition of calibrated amounts of InAs ML on clean GaAs(001) surfaces in a molecular-beam-epitaxy (MBE) chamber attached to the x-ray scattering facility. However, it will be shown that the results can be extended to the case of samples prepared by encapsulating an InAs monolayer under a GaAs cap. After chemical deoxidation performed in a solution of Ethanol- 10% HCl, semi-insulating GaAs samples designed for surface diffraction measurements ($13\times13\times2.5$ mm^3 with 45° beveled sides) were introduced into the MBE chamber. Annealing to 600 °C under an As_4 base pressure of a few 10^{-6} mbar produced a low background reflection high-energy electron-diffraction (RHEED) pattern with faint three-dimensional features in the $[1\bar{1}0]$ azimuth. A buffer layer, a few hundred nm thick, was then grown under standard conditions ($T_s=580$ °C, 0.2 nm/s), and a sharp (2×4)-reconstructed surface was obtained. Further smoothing was achieved by annealing to induce the 4×2 transition and cooling under an As_4 flux to the temperature selected for InAs deposition. The desired fraction of InAs ML was then deposited (after calibration of the indium flux using RHEED oscillations) either on a (2×4)- or $c(4\times4)$-reconstructed surface at ±10 °C from the transition temperature between the two reconstructions, i.e., about 500 °C under this arsenic flux. Figure 1 summarizes the preparation conditions of the eight samples discussed in this paper, and shows the conditions under which each structure was found. After indium deposition, the high-temperature samples (labeled 1–4 in Fig. 1) were cooled under the As flux to 350 °C, and then transferred under vacuum to the diffractometer stage. Samples prepared directly on the $c(4\times4)$ surface (labeled 5–8) were quenched in vacuum and some annealed to 250 °C (samples 7 and 8), a procedure which improves the surface ordering as revealed by the sharpening of the RHEED pattern.[9]

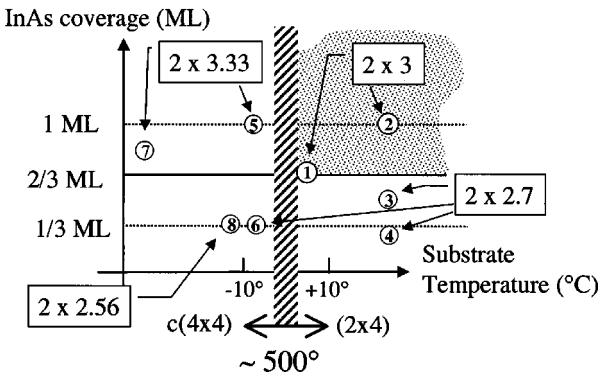

FIG. 1. Schematic diagram of the surface reconstructions observed as a function of the InAs deposited amount and substrate temperature. The preparation conditions for the samples discussed in the text are referred to by the labels 1–8.

Careful monitoring of the RHEED pattern after deposition showed that stable $2\times n$ reconstructions, where the value of n was time independent, could only be obtained for deposition temperatures on the lower side of the range displayed in Fig. 1. This enabled a study of the incommensurate surfaces from $n=2.55$ to 3.3 to be performed. In the high-temperature regime, particularly on the 2×4 templates, the InAs depositions in excess of the nominal $[\mathrm{In}]_s=\frac{2}{3}$ lead to the formation of the commensurate 2×3 reconstruction (sample 2), and those with a large indium deficit (0.25 ML deposited) started with an incommensurability of about 2×2.5 and evolved toward 2×2.7 in a few minutes (sample 4). These observations will be discussed in terms of the surface structures proposed. A somewhat intermediate behavior was also observed on the higher-temperature side of the $c(4\times4)$ surface reconstruction (samples 5 and 6).

B. Diffraction data collection

X-ray data have been recorded on the *W*12 beamline of the LURE-DCI synchrotron radiation facility, equipped with a double-crystal monochromator, sagitally focusing in the horizontal plane, and an ultrahigh-vacuum six-circle diffractometer coupled to the MBE growth chamber. Photons of 13 or 14 keV, incident on the sample, were aligned under grazing incidence at the critical angle for total external reflexion.

Data have been collected using two different schemes. Firstly, for the $In_xGa_{1-x}As$ commensurate phase, where diffracted intensities are expected to occur at in-plane Bragg positions and along the rods normal to the surface, a full set of data has been collected to complete the previously obtained in-plane measurements.[6] This allowed experimental assignment of the x, y, and z coordinates of the atoms in the surface unit cell. For the incommensurate phases, a continuous intensity distribution was expected in the direction of the discommensuration (k reciprocal axis), thus k scans were recorded along several reciprocal rows ($h=$const), together with accompanying scans performed with offsets $\pm\Delta h$ for a more accurate estimate of the background level. To assert the

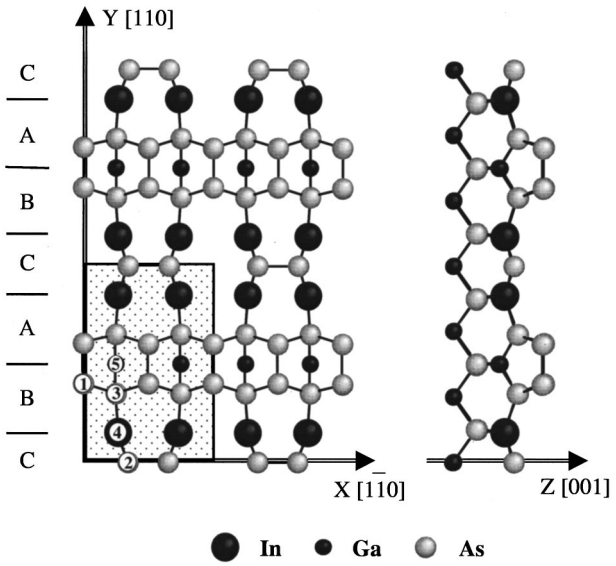

FIG. 2. Top and side views of the atomic structure for the commensurate 2×3 reconstruction. Labels refer to the atoms listed in Table I.

validity of the procedure, the results have been compared to a series of integrated transverse h scans recorded along the selected reciprocal row. Fractional diffraction rods were also collected in the incommensurate phases confirming the basic similarity of the atomic distribution on all these surfaces. Reflection indices refer to the (1×1) bulk derived surface cell with basis vectors

$$\mathbf{a}=\tfrac{1}{2}[1\bar{1}0]_{\text{cubic}},\quad \mathbf{b}=\tfrac{1}{2}[110]_{\text{cubic}},\quad \mathbf{c}=[001]_{\text{cubic}}.$$

III. RESULTS AND DISCUSSION

The atomic distributions in the surface layers of both commensurate and incommensurate phases have been derived from the x-ray data on the basis of an original formulation of the surface diffuse scattering.

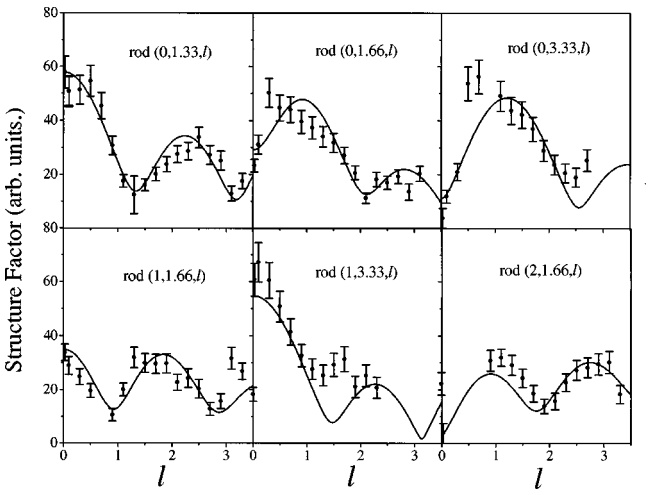

FIG. 3. Fractional rods measured in the commensurate phase: comparison between the experimental and calculated structure factors.

A. 2×3 commensurate phase

Since the structural elements present in the commensurate phase are building blocks for all types of $2\times n$ incommensurate surfaces, the 2×3 surface unit cell will be recalled first. The structural model, shown in Fig. 2, was deduced from in-plane surface x-ray-diffraction data and bond-length conservation hypothesis.[6] It has been fully confirmed by analysis of the present data set, and the experimentally determined atomic position parameters, both in and out of plane, are listed in Table I. It should also be noted that the z coordinates deduced from the rod scan fitting (Fig. 3) confirm the results of total-energy calculations previously made on the local indium bonding.[11] The surface structure of the 2×3 reconstruction can be described as follows.

(i) A ribbonlike feature extending in the $[1\bar{1}0]$ direction with chemisorbed arsenic dimers along [110], trapping two gallium atoms per unit cell in the third layer, this feature occupies two bulk lattice constants and will be referred to as the *AB* building block.

TABLE I. (a) Atomic coordinates derived from the best fit of the x-ray-diffraction data and referred to the 2×3 unit cell with $2a=7.9940$ Å, $3b=11.991$ Å, $c=5.6526$ Å, and $\alpha=\beta=\gamma=90°$. (b) Bond length (in Å).

(a)

Atom	X	Y	Z	Mult.[a]	Remark
As(1)	0	0.398 ± 0.004	$0.50+0.019\pm0.005$	4	
As(2)	$0.25+0.093\pm0.004$	0	$0.25+0.134\pm0.005$	4	
As(3)	0.25	$0.333+0.017\pm0.004$	$0.25+0.025\pm0.005$	2	
In(4)	$0.25+0.017\pm0.004$	$0.167-0.016\pm0.004$	$0.0+0.063\pm0.005$	4	
Ga(5)	0.25	0.5	0.0	2	Bulk position

(b)

Dimer	2.51
Chemisorbed dimer	2.44
As(1)-As(3)	2.49
As(3)-In(4)	2.69
As(3)-Ga(5)	2.40
As(2)-In(4)	2.63

[a]Number of symmetry-related items.

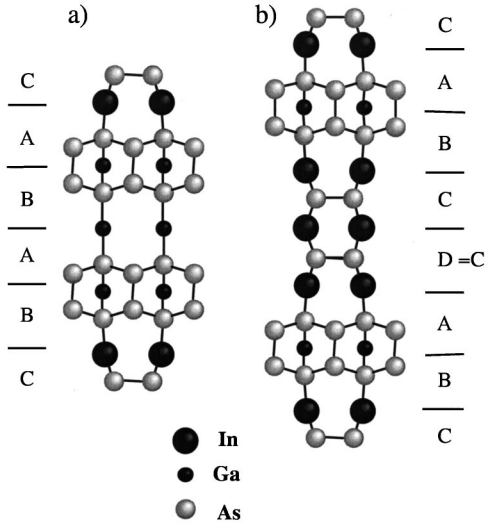

FIG. 4. Examples of faulted sequences for (a) an indium-depleted surface where one block *C* has been removed, and atoms at the faulted *BA* junction are taken as gallium; and (b) an indium-enriched surface showing the faulted *CC* pair.

(ii) Arsenic dimers aligned along the $[1\bar{1}0]$ direction, bonded to four indium atoms per unit cell; this structural element extends over one bulk lattice constant and will be referred to as the *C* block.

The ordered distribution of the cations in the 2×3 cell locks the surface composition on the value $In_{2/3}Ga_{1/3}As$ thus explaining the $[In]_s=0.7$ deduced by the spectroscopic measurements quoted above.

B. Model for the diffuse scattering from the incommensurate phases

The occurrence of $2\times n$ incommensurate phases with $n<3$ has already been correlated with an indium-depleted surface layer and an attempt to model the structure, by randomly suppressing the indium-rich block *C*, gave a satisfactory agreement with preliminary data collected on these surfaces.[6] Similarly one can think of the $2\times n$ incommensurate phases with $n>3$, obtained here by forcing the $[In]_s$ above $\frac{2}{3}$, as built with randomly distributed *CC* pairs of In-rich blocks, labeled *CD* to keep track of the difference between the unfaulted *C* and the faulted *D* blocks. Figure 4 is a schematic of these two types of faulted surfaces. The limiting cases where, on the one hand, all the *C* blocks are removed leads to the pure GaAs $c(4\times4)$ surface provided that every fourth chemisorbed As dimer is deleted. By contrast, when all *C* blocks are replaced by *CD* pairs, one obtains a As-rich 2×4 reconstruction which has indeed been observed on $In_{0.53}Ga_{0.47}As$ alloys grown lattice matched on InP.[12] This section will be dedicated to a detailed calculation of the expected diffuse scattering distribution for both types of faulted surfaces, and the comparison with the experimental data will be presented in Sec. III C.

In the framework of diffuse scattering formalism,[13] the scattering amplitude can be expressed by the formula

$$A(\mathbf{q})=\sum_{N=-\infty}^{\infty} F_N \exp(-i\mathbf{q}\cdot\mathbf{R}_N), \tag{1}$$

where the summation is performed over all the blocks N located at the extremity of the vector $R_N=2u\mathbf{a}+v\mathbf{b}$, where u and v are integers ($2\mathbf{a}$ and $\mathbf{b}$ being the dimension of individual blocks in the surface description), and $\mathbf{q}$ is the scattering vector defined as $\mathbf{q}=2\pi(s-s_0)/\lambda$, where $\mathbf{s}_0$ and $\mathbf{s}$ are unit vectors in the directions of the incident and scattered beams. The term F_N, the structure factor of the Nth block, is expressed as $F_N=\Sigma_j f_j \exp(-i\mathbf{q}\cdot\mathbf{r}_j)$, where the summation is performed over all atoms in the block, and f_j is the scattering factor of the jth atom located by the vector $\mathbf{r}_j$.

In the single scattering kinematic approximation, valid here because of the weak interaction between high-energy photons and electrons, the diffracted intensity takes on the form

$$\begin{aligned} I(\mathbf{q})=|A(\mathbf{q})|^2&=\sum_{M=-\infty}^{\infty}\langle F_N F_{N+M}^*\rangle_N \exp(i\mathbf{q}\cdot\mathbf{D}_M)\\ &=2\,\mathrm{Re}\left[\sum_{M=1}^{\infty}\langle F_N F_{N+M}^*\rangle_N \exp(i\mathbf{q}\cdot\mathbf{D}_M)\right]\\ &\quad+\langle F_N F_N^*\rangle_N, \end{aligned} \tag{2}$$

where $\mathbf{D}_M=\mathbf{R}'_N-\mathbf{R}_N$ is the vector separation between the N'th and Nth blocks ($M=N'-N$). The notation $\langle\ \rangle_N$ indicates that the average value of the structure factor product for blocks separated by the vector $\mathbf{D}_M$ is taken over all possible locations $\mathbf{R}_N$. This quantity, also referred to as the pair-correlation function, can be expressed in terms of the pair probabilities $P_{XY}(M)$ for a block X to have a block Y as Mth neighbor. This gives

$$\langle F_N F_{N+M}^*\rangle_N=\sum_X\sum_Y c_X P_{XY}(M) F_X F_Y^*, \tag{3}$$

where c_X is the surface concentration of block X, X, and Y standing for the different states A–D.

The case of indium depleted layers will be considered before the calculations are extended to include the indium rich surfaces. In both cases, the problem will be considered as unidimensional since the fault distribution concerns only the y direct axis and thus the k reciprocal axis.

Case A: indium-depleted layers reconstructed $2\times n$ for $n<3$. Let p_- be the probability of finding a *C* block between unbreakable *AB* pairs. The limiting value for p_- is 1 for *ABCABC...*, a sequence corresponding to the commensurate 2×3 arrangement and 0 for *ABAB...*, a pseudo 2×2 mimicking the $c(4\times4)$ reconstruction. With a given propagation direction, namely, *B* always following *A* and *C* following *B* with the probability p_-, the nearest-neighbor pair probabilities are expressed as

$$\begin{aligned} &P_{AA}(1)=0,\quad P_{BA}(1)=1-p_-,\quad P_{CA}(1)=1,\\ &P_{AB}(1)=1,\quad P_{BB}(1)=0,\quad P_{CB}(1)=0,\\ &P_{AC}(1)=0,\quad P_{BC}(1)=p_-,\quad P_{CC}(1)=0. \end{aligned} \tag{4}$$

The propagation of this relation from the $P_{XY}(M)$ to the $P_{XY}(0)$ leads to the matrix equation

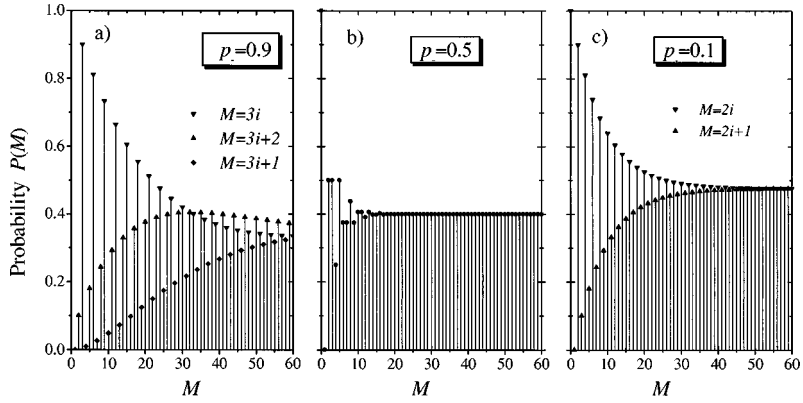

FIG. 5. Pair probability for identical Mth neighbors: $P_{AA}(M)=P(M)$ for different fault probability p_-. (a) $p_-=0.9$; the decay length of the $\times 3$ long range order is clearly evidenced by sampling with $M=3i$. (b) $p_-=0.5$; no correlations appear. (c) $p_-=0.1$; the tendency toward a $\times 2$ ordering is demonstrated on the $M=2i$ sampling.

$$\begin{pmatrix} P_{AA}(M) \\ P_{AB}(M) \\ P_{AC}(M) \end{pmatrix} = \begin{pmatrix} 0 & 1-p_- & 1 \\ 1 & 0 & 0 \\ 0 & p_- & 0 \end{pmatrix} \begin{pmatrix} P_{AA}(M-1) \\ P_{AB}(M-1) \\ P_{AC}(M-1) \end{pmatrix} = \begin{pmatrix} 0 & 1-p_- & 1 \\ 1 & 0 & 0 \\ 0 & p_- & 0 \end{pmatrix}^M \begin{pmatrix} P_{AA}(0)=1 \\ P_{AB}(0)=0 \\ P_{AC}(0)=0 \end{pmatrix}, \quad (5)$$

with the origin chosen on a block A. Equation (5) can be solved by standard matrix algebra, and leads to the expression

$$P_{AA}(M)=P(M)=\frac{1}{2+p_-}\{1+A_+\lambda_+^{M+2}+A_-\lambda_-^{M+2}\} \quad \text{for } M>0, \quad (6)$$

with

$$\lambda_{+,-}=\frac{-1\pm\sqrt{1-4p_-}}{2} \quad \text{and} \quad A_{+,-}=\frac{-1}{2}\pm\frac{-3}{2\sqrt{1-4p_-}}. \quad (7)$$

It should be remarked that for $p_-<\frac{1}{4}$ the solutions are no longer real.

The variation with M of the pair probability $P(M)$ for Mth neighbors to be identical, is an optimal flag to estimate the measure and range of the periodicity on the surface. For $p_-=1$, $P(M)=1/3(1+j^{M+3}+\bar{j}^{M+3})$ with $j=e^{i2\pi/3}$ and $\bar{j}=e^{-i2\pi/3}$ which means that $P(M)=1$ when M is multiple of 3 and $P(M)=0$ otherwise, one recognizes the $\times 3$ periodicity with respect to the bulk basis, i.e., the commensurate 2×3 structure. In the other limiting case, $p_-=0$, $P(M)=1/2[1+(-1)^{M+2}]$ leading to $P(M)=1$ when M is multiple of 2 and $P(M)=0$ otherwise, which describes the $\times 2$ periodicity of the pseudo $c(4\times 4)$ structure.

$P(M)$ is presented in Figs. 5(a)–5(c) for three intermediate values.

(a) $p_-=0.9$ the sampling of $P(M)$ for $M=0$, 1, or 2 mod(3) shows the dominance of a $\times 3$ periodicity up to $M=25$, whereas the probability to find identical blocks in faulted sites increases with M, the limiting pair probability value for large M is the surface concentration of A blocks, namely, 1/2.9 in this case.

(b) $p_-=0.5$ long-range order can no longer be detected in the AB and C block distributions.

(c) $p_-=0.1$ $P(M)$ is dominated for small M by the $\times 2$ periodicity.

In the same way as in strictly periodic systems, the intensity distribution in reciprocal space is governed by the Fourier transform of the direct lattice, it can be anticipated that in the present case, the shape of the diffuse scattering will be determined by the Fourier transform of $P(M)$. Figure 6(a) shows the evolution of $TF[P(M)]$ for a series of values of p_- along one bulk reciprocal-lattice period in the **b*** direction. Two maxima, progressively broadened and shifted from the commensurate positions ($k=\frac{1}{3}$ and $\frac{2}{3}$) are observed as p_- decreases. Below $p_-=0.25$ the two maxima eventually merge into a single peak centered at $k=\frac{1}{2}$.

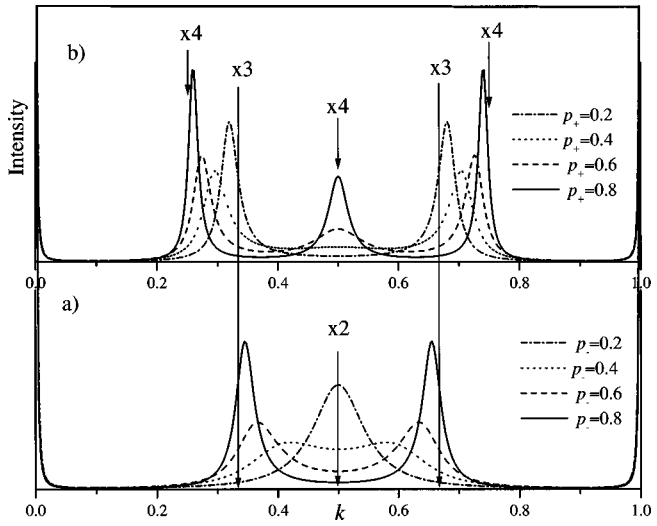

FIG. 6. Fourier transform of $P(M)$ along a **b*** reciprocal-lattice period for a series of p_- and p_+ values. (a) For indium-depleted surfaces, peaks are seen to shift inward from the commensurate positions ($\frac{1}{3},\frac{2}{3}$) leading to $2\times n$ surfaces with $2<n<3$ (b) In the indium-enriched case, peaks shift outward until eventually a $\times 4$ periodicity emerges.

Due to the nearest-neighbor constraints, the pair probabilities propagate with M in the following way:

$$P_{XY}(M)=\sum_Z P_{XZ}(1)P_{ZY}(M-1)$$

and

$$P_{XY}(M)=\sum_Z P_{XZ}(M-1)P_{ZY}(1). \tag{8}$$

All $P_{XY}(M)$ can be expressed as a function of one of them, $P(M)$, according to

$$P_{AA}(M)=P(M),\quad P_{BA}(M)=P(M+1),\quad P_{CA}(M)=P(M-1),$$
$$P_{AB}(M)=P(M-1),\quad P_{BB}(M)=P(M),\quad P_{CB}(M)=P(M-2),$$
$$P_{AC}(M)=p_-P(M-2),\quad P_{BC}(M)=p_-P(M-1),\quad P_{CC}(M)=p_-P(M-3). \tag{9}$$

Introducing these values in formula (2), and taking into account that the fault propagation takes place only along the **b** axis of the direct lattice with $\mathbf{D}_M=M\mathbf{b}$, the intensity distribution can be described by the expression

$$\begin{aligned}I(q_y)\propto 2\,\mathrm{Re}\Bigg[\sum_{M=1}^{\infty}P(|M|)e^{iMq_y}\{&F_AF_A^*+F_BF_B^*+F_AF_B^*e^{iq_y}+F_BF_A^*e^{-iq_y}+p_-^2F_CF_C^*e^{3iq_y}\\&+p_-(F_AF_C^*e^{2iq_y}+F_CF_A^*e^{iq_y}+F_BF_C^*e^{iq_y}+F_CF_B^*e^{2iq_y})\}\Bigg]\\&+2\,\mathrm{Re}[F_AF_B^*e^{iq_y}+p_-(F_AF_C^*e^{2iq_y}+F_CF_A^*e^{iq_y}+F_BF_C^*e^{iq_y}+F_CF_B^*e^{2iq_y}+p_-F_CF_C^*e^{3iq_y})]\\&+F_AF_A^*+F_BF_B^*+p_-F_CF_C^*,\end{aligned} \tag{10}$$

where $q_y=2\pi k$ is the variable along the **b*** reciprocal direction, and the structure factors are evaluated for the proper *hkl* values.

Case B: indium-rich layers reconstructed $2\times n$ for $n>3$. A similar treatment can be applied to the case of indium rich surfaces.[14] Starting with the description sketched in Fig. 4(b), one introduces the probability p_+ of finding a D block after the now undissociated ABC sequence. It should be noticed that the commensurate 2×3 phase corresponds here to $p_+=0$. Nearest-neighbor constraints are then expressed as

$$P_{AA}(1)=0,\quad P_{BA}(1)=0,\quad P_{CA}(1)=1-p_+,\quad P_{DA}(1)=1,$$
$$P_{AB}(1)=1,\quad P_{BB}(1)=0,\quad P_{CB}(1)=0,\quad P_{DB}(1)=0,$$
$$P_{AC}(1)=0,\quad P_{BC}(1)=1,\quad P_{CC}(1)=0,\quad P_{CC}(1)=0,$$
$$P_{AD}(1)=0,\quad P_{BD}(1)=0,\quad P_{CD}(1)=p_+,\quad P_{CD}(1)=0,$$

which leads to a propagation matrix

$$\begin{pmatrix}P_{AA}(M)\\P_{AB}(M)\\P_{AC}(M)\\P_{AD}(M)\end{pmatrix}=\begin{pmatrix}0&0&1-p_+&1\\1&0&0&0\\0&1&0&0\\0&0&p_+&0\end{pmatrix}^M\begin{pmatrix}P_{AA}(0)=1\\P_{AB}(0)=0\\P_{AC}(0)=0\\P_{AD}(0)=0\end{pmatrix}. \tag{11}$$

The solution to Eq. (11) leads to

$$P_{AA}(M)=P(M)=\frac{1}{1+\lambda_0}\{A_0+A_1\lambda_0^{M+3}+A_+\lambda_+^{M+3}+A_-\lambda_-^{M+3}\}\quad\text{for } M>0, \tag{12}$$

where λ_0 is the unique real root of the polynomial $\lambda^3+\lambda^2+\lambda+p$, and

$$\lambda_\pm=\frac{1}{2}\{-(\lambda_0+1)\pm i\sqrt{3\lambda_0^2+2\lambda_0+3}\},$$

$$A_0=\frac{1}{(\lambda_+-1)(\lambda_--1)},$$

$$A_1=-\frac{1}{(\lambda_+-\lambda_0)(\lambda_--\lambda_0)},$$

$$A_\pm=\pm\frac{1}{(\lambda_+-\lambda_-)(\lambda_\pm-\lambda_0)(\lambda_\pm-1)}.$$

Starting with a 4×4 matrix, the resolution of the eigenvalue equation is somewhat more tedious; nevertheless a solution is possible, and one obtains an expression for the intensity distribution containing the Fourier transform of $P(M)$. Fig-

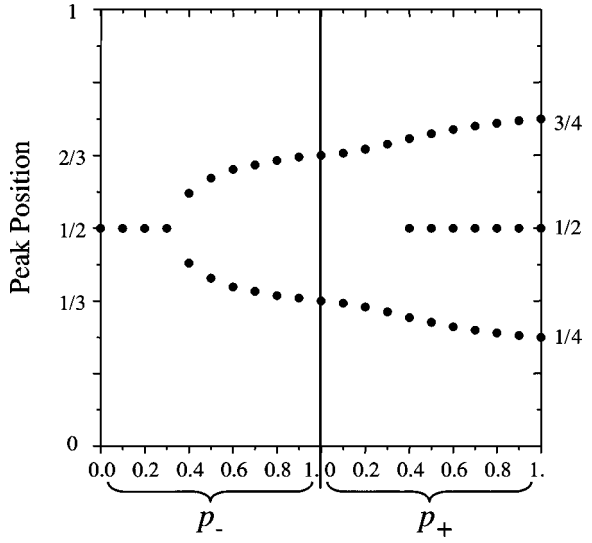

FIG. 7. Calculated peak positions as a function of the fault probability in both cases.

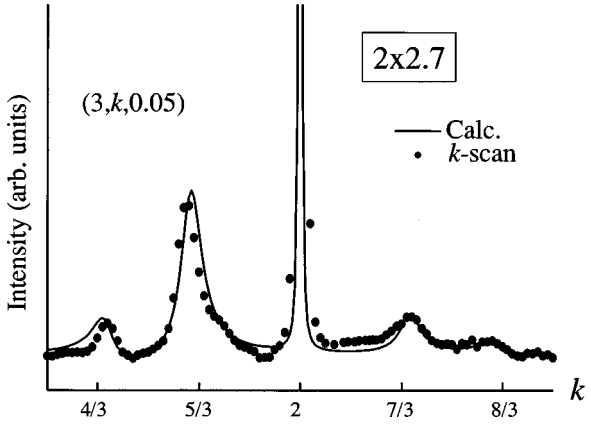

FIG. 8. Comparison between the experimental intensity (background subtracted) measured in sample 3 along the reciprocal row (3,k,0.05), and the distribution calculated from formula (10). The only free parameter is the fault probability p_- adjusted at 0.6. The derived indium surface concentration is $[\mathrm{In}]_s = 0.45$

ure 6(b) displays its variation for a set of p_+ values. As p_+ increases, the two maxima are seen first to broaden and shift outward from the commensurate $\times 3$ positions and eventually to evolve into the three sharp peaks of a new $\times 4$ commensurate phase.

For both types of surfaces, the peak position which is the most readily obtained experimental information, for instance from the RHEED pattern, appears directly connected to the $p_\pm$ value as illustrated in Fig. 7. From the atomic models proposed in Fig. 4, one is able to derive the following relations between the fault probabilities and the indium surface concentrations where the proper weights have been used for the Ga and In atoms at the faulted boundaries:

$$[\mathrm{In}] = \frac{2p_-}{2+p_-}$$

in indium-depleted surfaces, and

$$[\mathrm{In}] = \frac{2+p_+}{3+p_+}$$

in indium-enriched surfaces. A quick access to this key property of the investigated ternary system is therefore available.

In order to obtain a full simulation of the expected intensity, one should calculate the total expressions according to Eq. (10), and its equivalent for the In-rich case. As a consequence, the schematic distributions shown in Figs. 6(a) and 6(b) will be modulated by the structure factor variations along the reciprocal row. Several experimental cases will now be presented.

C. Comparison between experimental data and simulations

Case A: Indium-depleted layers $2\times n$ for $2.5<n<3$. Such layers are first prepared on the GaAs 2×4 surface at around 520–530 °C. In the example of sample 3 in Fig. 1, 0.5-ML InAs were deposited. An incommensurate 2×2.7 reconstruction was obtained after cooling under an As flux down to 350 °C. The background-subtracted continuous k scan ($1<k<3$) recorded along the $h=3$ reciprocal row is displayed in Fig. 8 together with the expected intensity derived from Eq. (10), where the probability p_- has been taken equal to 0.6. Good agreement is obtained for the peaks positions, heights, and widths. The estimated indium surface concentration is 0.45, a value compatible with the deposited amount when considering the calibration uncertainty.

A similar intensity distribution could equally be observed after encapsulation of 1-ML InAs under 6 ML of GaAs in the same temperature range,[15] as shown in Fig. 9, where the experimental k scans recorded along the same reciprocal row in the two different samples are presented. Such a result not only demonstrates the generality of this type of reconstruction, but also could provide a way to estimate the In concentration profile in the diffuse interface region. In addition, the discrete measurements obtained by integrating a series of transverse h scans along the same reciprocal row are superimposed on the continuous k scan for the encapsulated sample. The similarity of the intensity variation assesses the validity of the much less time-consuming k scan data collection procedure for such studies.

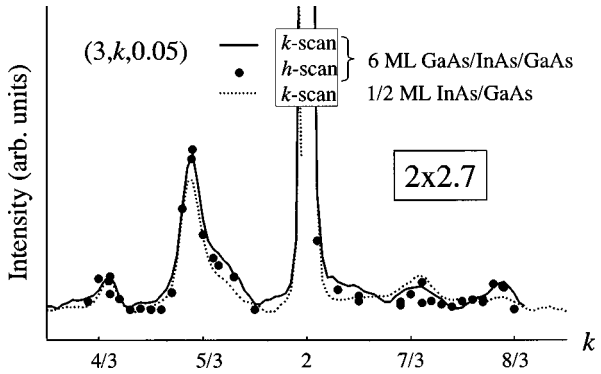

FIG. 9. Experimental data recorded with samples prepared in two different conditions but showing the same surface concentration of indium: the k scan in sample 3 was already presented in Fig. 8 (0.5-ML InAs/GaAs 2×4); k scan and series of integrated transverse h scans on a sample prepared by burying 1-ML InAs under 6-ML GaAs at 530 °C.

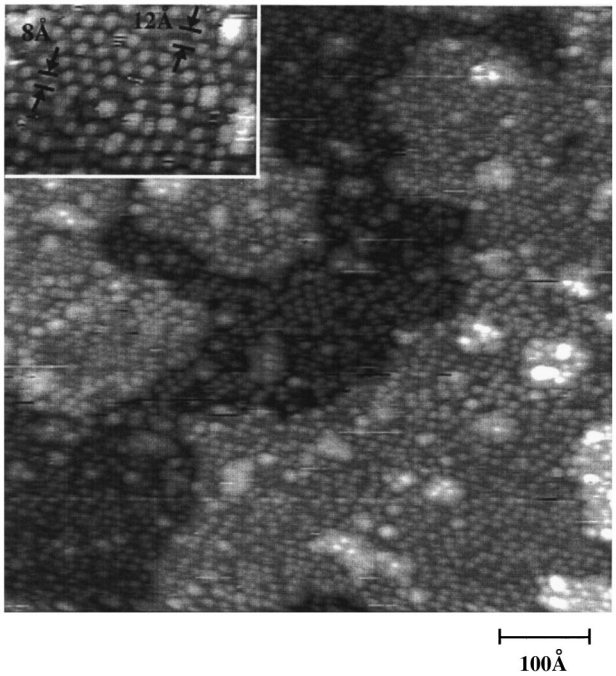

FIG. 10. STM image showing a single-phase surface with a low indium coverage obtained by depositing 0.3-ML InAs at 470 °C (after Ref. 9).

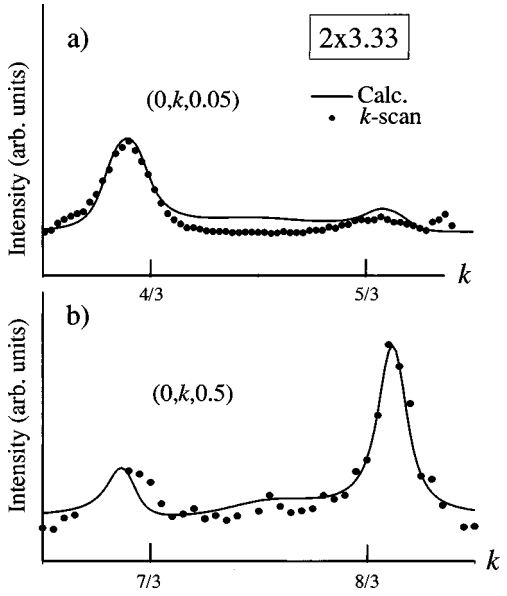

FIG. 11. Two examples of indium-enriched surfaces: (a) sample 7 and (b) sample 5. The best fit value for p_+ in both cases is 0.55, corresponding to the 2×3.33 reconstruction, and leading to a surface concentration of indium of 0.7.

It should be noted that in this deposition temperature range, highly incommensurate surfaces could not be stabilized. For instance after depositing 0.25 ML of InAs (sample 4 in Fig. 1), the RHEED pattern observed in real time on cooling under the As flux turned from a quasi 2×2.5 surface to a 2×2.7 after a few minutes. Since laterally homogeneous surfaces are expected at this temperature,[16] this could only be related to a reduced driving force for cation ordering within the arsenic-controlled superstructure.

By contrast, these surfaces could be stabilized when produced on the $c(4\times4)$-reconstructed substrates, as was the case for sample 8 prepared around 470 °C. These results are in full agreement with previous STM observations,[9] in which homogeneous surfaces with a distributed density of faults were observed in such coverage and temperature regime (Fig. 10). The transition between the two regimes should occur around 490 °C since sample 6, where the same low coverage was deposited, could not be stabilized at $n=2.5$ and evolved toward $n=2.7$, as was observed with sample 4. The strict correspondence between surface concentration and discommensuration is thus lost above approximately 500 °C.

Case B: Indium-rich surfaces $2\times n$ with $n>3$. As mentioned in Sec. I such incommensurate surfaces could only be obtained on $c(4\times4)$ substrates. The two examples displayed in Figs. 11(a) and 11(b) were prepared using slightly different conditions: for sample 5, 1-ML InAs was deposited at the upper temperature limit of the $c(4\times4)$ surface, whereas, for sample 7, deposition of about 0.8-ML InAs was performed at 450 °C. An identical 2×3.33 incommensurate surface was observed in both cases, and the experimental intensities recorded along $[0,k,0.5]$ with $2<k<3$ for sample 5 [Fig. 11(a)], and along $[0,k,0.05]$ with $1<k<2$ for sample 7 [Fig. 11(b)], are in good agreement with the calculations. The fault probability derived from the best adjustment is $p_+=0.4$, which corresponds to a surface concentration of indium $[\mathrm{In}]_s$ equal to 0.7. It should be remarked that the highest concentration attainable within this fault model would be 0.75 for the commensurate 2×4 surface. Due to the epitaxial strain, it appears that a larger amount of In cannot be incorporated in a single layer. A comparison with the STM images obtained in the same preparation conditions (Fig. 2d in Ref. 9) shows that the surfaces are indeed homogeneously $2\times n$ reconstructed, no bare $c(4\times4)$ areas can be detected and broad two-dimensional islands are present. Careful inspection allows identification of a $\times4$ local periodicity between the chemisorbed As white features in the lower terraces.

IV. CONCLUSIONS

A satisfactory account of the incommensurate $2\times n$ surfaces obtained in the ternary system $\mathrm{In}_x\mathrm{Ga}_{1-x}\mathrm{As}$, when fully strained on a GaAs(001) substrate, has been obtained by introducing a statistical distribution of defects corresponding to a locally In-depleted or -enriched surface with respect to the commensurate 2×3 $\mathrm{In}_{2/3}\mathrm{Ga}_{1/3}\mathrm{As}$-ordered surface alloy. Such an approach enables us to put figures on the actual surface concentration in homogeneous cases where a mere description by a mixture of commensurate limiting phases would be inappropriate. The occurrence of incommensurate reconstructions is quite frequent in semiconductor materials, for instance a quasicontinuous transition between 2×1 and 3×1 structures, observed by dosing GaAs with Si during epitaxial growth, has been studied both by RHEED STM (Ref. 17) and low energy electron diffraction.[18] Although a model was proposed for the Si-atom location, a quantitative interpretation of the diffuse intensity distribution was not attempted on this surface. The mathematical treatment presented here is based on the existence of an underlying

1×1 bulk structure which forces the building blocks for the ''imperfect'' structure to be of unit length. It can be easily understood that beyond four blocks, the problem becomes mathematically intractable. A more general treatment involving a statistical distribution of blocks of any length was proposed by Croset and De Beauvais[19] for incommensurate adsorbates on graphite, and has indeed been applied to large incommensurate $2\times n$ Bi/Si(001) interfaces.[20]

ACKNOWLEDGMENTS

We are indebted to B. Croset and C. De Beauvais who made their unpublished results available to us. Upgrading of the LURE surface diffraction beamline was performed under EC Contract No. CI1*CT93-0034. Financial support from the EPSRC (UK) and the National University of Singapore for E.S.T. is gratefully acknowledged.

*Author to whom correspondence should be addressed. FAX: 33 1 64 46 41 48. Electronic address: garreau@lure.u-psud.fr

[1] W. Hebenstreit, G. Ritz, M. Schmid, A. Biedermann, and P. Varga, Surf. Sci. **388**, 150 (1997).
[2] J. M. Moison, C. Guille, F. Houzay, F. Barthe, and M. Van Rompay, Phys. Rev. B **40**, 6149 (1989).
[3] J. Nagle, J. P. Landesman, M. Larive, C. Mottet, and P. Bois, J. Cryst. Growth **127**, 550 (1993).
[4] K. Muraki, S. Fukatsu, Y. Shiraki, and R. Ito, Appl. Phys. Lett. **61**, 557 (1992).
[5] J. M. Gerard and J. Y. Marzin, Phys. Rev. B **45**, 6313 (1992).
[6] M. Sauvage-Simkin, Y. Garreau, R. Pinchaux, M. B. Véron, J. P. Landesman, and J. Nagle, Phys. Rev. Lett. **75**, 3485 (1995).
[7] M. Sauvage-Simkin, Y. Garreau, R. Pinchaux, A. Cavanna, M. B. Véron, N. Jedrecy, J. P. Landesman, and J. Nagle, Appl. Surf. Sci. **104/105**, 646 (1996).
[8] J. M. Moison, C. Guille, and M. Bensoussan, Phys. Rev. Lett. **58**, 2555 (1987).
[9] J. C. Belk, J. L. Sudijono, D. M. Holmes, C. F. McConville, T. S. Jones, and B. A. Joyce, Surf. Sci. **365**, 735 (1996).
[10] J. C. Belk, C. F. McConville, J. L. Sudijono, T. S. Jones, and B. A. Joyce, Surf. Sci. **387**, 213 (1997).
[11] L. Bellaïche, K. Kunc, M. Sauvage-Simkin, Y. Garreau, and R. Pinchaux, Phys. Rev. B **53**, 7417 (1996).
[12] K. Aïd, Y. Garreau, M. Sauvage-Simkin, and R. Pinchaux (unpublished).
[13] T. R. Welberry, Rep. Prog. Phys. **48**, 1543 (1985).
[14] H. Moussa, M. S. dissertation, LURE, University Paris-sud, 1996.
[15] M. Delmas, M. S. Dissertation, LURE, University Paris VI, 1995.
[16] J. M. Gérard, J. Cryst. Growth **127**, 981 (1993).
[17] A. R. Avery, J. L. Sudijono, T. S. Jones, and B. A. Joyce, Surf. Sci. **340**, 57 (1995).
[18] A. H. Levermann, D. A. Woolf, D. I. Westwood, and J. E. Macdonald, Surf. Sci. **352–354**, 812 (1996).
[19] B. Croset and C. De Beauvais, Surf. Sci. **409**, 403 (1998).
[20] N. Jedrecy, L. Gavioli, M. G. Betti, C. Mariani, B. Croset, and C. De Beauvais (unpublished).